Chemical Vapor Deposition

Full Paper

# $Bi_{1-x-y}Ti_xSi_yO_z$ (BTSO) Thin Films for Dynamic Random Access Memory Capacitor Applications**

By *Yo-Sep Min*,* *Young Jin Cho*, *Igor P. Asanov*, *Jeong Hee Han*, *Wan Don Kim*, and *Cheol Seong Hwang*

$Bi_{1-x-y}Ti_xSi_yO_z$ (BTSO) thin films were grown on eight inch diameter $Ru/SiO_2/Si$ or bare Si wafers by atomic layer deposition (ALD) method using $Bi(mmp)_3$, $Ti(mmp)_4$, and $Si(OEt)_4$ [mmp = 1-methoxy-2-methyl-2-propoxide ($OCMe_2CH_2OMe$, Me = methyl); Et = ethyl] as metal alkoxide precursors and ozone ($O_3$) as the oxidant gas. Transmission electron microscopy (TEM) and Rutherford backscattering spectrometry (RBS) analysis showed that the as-deposited films are amorphous and the cation compositional ratio of Bi:Ti:Si is 0.38:0.37:0.25 of films deposited at 325 °C on $Ru/SiO_2/Si$ Ru substrates. X-ray photoelectron spectroscopy (XPS) shows that the BTSO films are homogeneously dispersed without any phase-separation of the components. The BTSO films show excellent step coverage on a high aspect ratio (4) contact hole structure with a diameter of 300 nm. The leakage current density of BTSO films is on the order of $10^{-8}$ A cm$^{-2}$ at 1 V, meeting present dielectric requirements for a dynamic random access memory storage capacitor with an equivalent oxide thickness of 2.1 nm. From the capacitance–voltage characteristics at 10 kHz of the Pt/BTSO/Ru capacitor, the estimated dielectric constant of amorphous BTSO films is ~24.

Keywords: ALD, BTSO, Capacitor, DRAM, High-*k* dielectrics

## 1. Introduction

As the density of dynamic random access memory (DRAM) quadruples every three years, dielectric layers with a higher dielectric constant (high-*k*) must be adopted in the storage capacitor in order to maintain sufficient cell capacitance (> 30 fF per cell) with ever-shrinking capacitor sizes.[1] Recently, $HfO_2$ and $Ta_2O_5$ thin films have attracted great attention as promising high-*k* dielectrics for metal/insulator/silicon (MIS) and metal/insulator/metal (MIM) capacitors, respectively.[2] The International Technology Roadmap for Semiconductors (ITRS) forecasts barium strontium titanate ($(Ba,Sr)TiO_3$, BST) thin films with higher dielectric constants ($k > 250$) to replace $Ta_2O_5$ ($k > \sim 60$) in gigabit density DRAMs within several years.[1c] However, metal–organic (MO)CVD of BST thin films have not been successful even with the extensive research work in the 1990s.[3] The difficulties primarily originate from the low volatility and instability of Group II element (Ba, Sr) precursors due to the low charge-to-radius ratios of Ba and Sr ions[4] which makes the precursor delivery in the MOCVD process less reliable. Because Ba and Sr precursors usually have unoccupied coordination sites causing decomposition and/or oligomerization, the available Ba or Sr precursors for vapor phase deposition are mainly limited to $\beta$-diketonato complexes or Lewis base adducts of them.[4] In addition to the precursor issues, reducing the thickness of BST (< ~50 nm) thin films seriously deteriorates the dielectric constant when they are deposited on metal electrodes owing to the presence of intrinsic interfacial low dielectric layers and the electrode charging effect.[5] It should also be noted that a very thin thickness (< 15 nm) of the dielectric films must be used in DRAM capacitors due to the very small spacing (≪ 100 nm) between capacitor nodes. However, high-*k* thin films, such as BST, usually show an unacceptably high leakage current due to the small band gap (~ 3 eV) and high defect density. One more serious concern for the MOCVD process of BST films is the non-uniform cation composition ratio ((Ba+Sr):Ti) over three-dimensional capacitor node structures. It was found that the deposition of compositionally uniform BST films was possible but requires a specially tuned process recipe and dome-type MOCVD chamber that could heat the entire system to a high temperature.[6] However, this problem must be taken seriously when any multi-cation dielectric film is adopted as the DRAM capacitor dielectric.

Recently, $Bi_2Ti_2O_7$, which has a pyrochlore structure, has been studied as the capacitor dielectric for DRAM appli-

[*] Y. S. Min, Y. J. Cho, Dr. J. H. Han
Nano Fabrication Center, Samsung Advanced Institute of Technology
San 14-1, Nongseo-Ri, Kiheung-Eup
Yongin-City, Kyungki-Do, 449-712 (Korea)
E-mail: ysmin@sait.samsung.co.kr
Y. S. Min, W. D. Kim, Prof. C. S. Hwang
School of Materials Science and Engineering, Seoul National University
Seoul, 151-742 (Korea)
Dr. I. P. Asanov
Analytical Engineering Center
Samsung Advanced Institute of Technology
San 14-1, Nongseo-Ri, Kiheung-Eup
Yongin-City, Kyungki-Do, 449-712 (Korea)

[**] This work was partially supported by the System IC 2010 project of the Korean government.

  DOI: 10.1002/cvde.200406328 

cations, owing to its good insulating property and high dielectric constant.[7] The leakage current density of a $Bi_2Ti_2O_7$ film (600 nm thick is of the order of $10^{-7}$ A cm$^{-2}$ when the applied voltage is between – 18 V and + 18 V. The dielectric constant varies from 159 to 150, while the dissipation factor is < 0.02, within the frequency range of 10–100 kHz.[7c]

Atomic layer deposition (ALD), a technique developed in the 1970s, has just recently attracted great attention in the microelectronic industry, because of the low growth rate, normally slower than 1 Å per cycle.[8] ALD is a special modification of CVD to deposit thin films through self-limiting growth by surface adsorptions of precursors. The precursors for films are supplied by alternating pulses of metal precursors and reaction gas with purging steps between the pulses. Therefore, in an ALD process, thermal self-decompositions of the precursors on the growing surface and homogeneous reactions in gas phase are inherently avoided. The resulting films are very conformal and the thickness are precisely controlled by the process cycles.

To use multi-component oxides as a high-*k* dielectric, the film composition should be reproducibly and reliably adjusted during the deposition process. A "cocktail" of precursors in a single solution is often used to solve this problem. To evaporate the precursors from a single cocktail, each precursor should be vaporized at similar temperatures and be stable without any unfavorable reactions with other precursors or solvents in the precursor solution.[9] Jones et. al. reported that $Bi(mmp)_3$ and $Ti(mmp)_4$ (mmp = 1-methoxy-2-methyl-2-propoxide, $OCMe_2CH_2OMe$; Me = methyl) is the best matched and most suitable precursor combination for liquid injection CVD in the Bi-Ti system.[10] $Bi(mmp)_3$ and $Ti(mmp)_4$ show very similar vapor pressure of ~ 0.1 torr at 100 °C.

In this study, we investigated amorphous dielectric $Bi_{1-x-y}Ti_xSi_yO_z$ (BTSO) films as a dielectric for DRAM capacitors. Si atoms were added to $Bi_2Ti_2O_7$ in order to make the films amorphous. The material has a medium-*k* value (20–30) and an amorphous structure which makes the dielectric properties less sensitive to the film thickness. The ALD process was adopted in this study for depositing the BTSO films to obtain conformal deposition on a three-dimensional structure in terms of thickness and cation composition.

## 2. Results and Discussion

ALD of BTSO thin films was performed using a single cocktail solution of $Bi(mmp)_3$, $Ti(mmp)_4$, $Si(OEt)_4$ [mmp = 1-methoxy-2-methyl-2-propoxide ($OCMe_2CH_2$-OMe, Me = methyl); Et = ethyl], dissolved in ethylcyclohexane, with $O_3$ gas as the oxidant. Approximately 0.028 mL of the precursor solution was fed to the reaction chamber in one injection. BTSO thin films were deposited on both bare Si wafers and Ru (500 Å)/$SiO_2$ (450 Å)/Si substrates at the same time because thickness measurements using spectroscopic ellipsometry on the former are much easier than on the latter. Although Ru films are used as a bottom electrode for a capacitor, ALD process conditions were determined from the results of the depositions on Si wafers.

Figure 1a shows the variation in growth rate ($G_r$) as a function of deposition temperature ($T_{dep}$). $G_r$ increases with

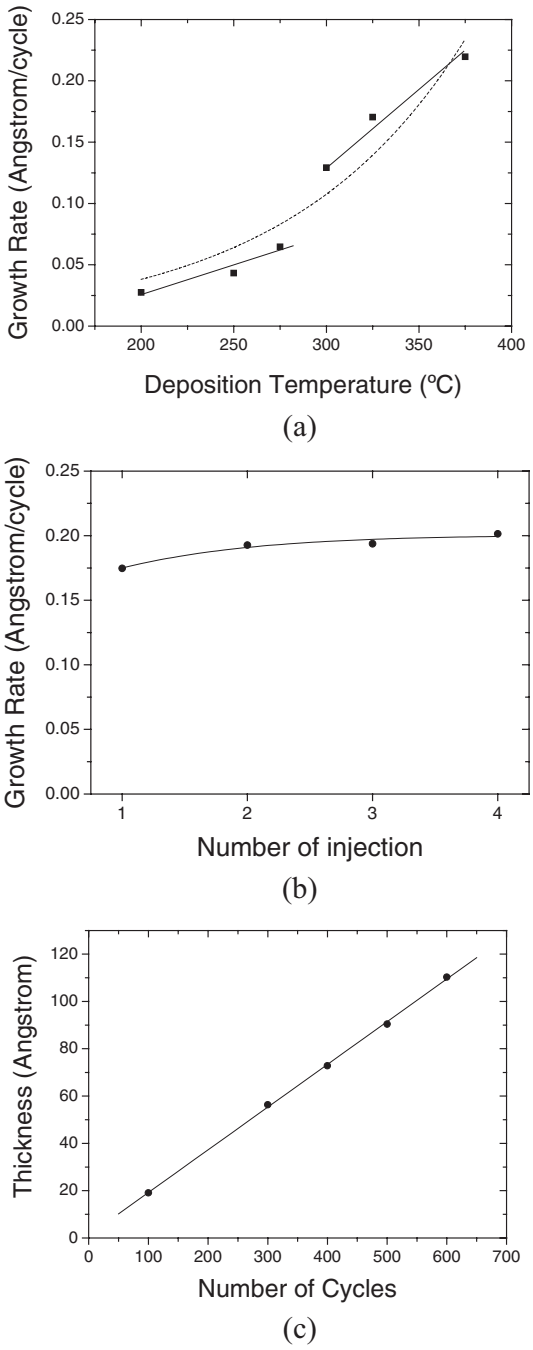


Fig. 1. a) Dependence of BTSO film growth rate ($G_r$) on deposition temperature ($T_{dep}$) (purge–source–purge–$O_3$ = 5–4–5–3 [s]; 1 injection; 500 cycles; Si wafer). b) Growth rate as a function of number of precursor injection. (purge–source–purge–$O_3$ = 5–4–5–3 [s]; 500 cycles; 325 °C; Si wafer). c) The thickness linearity with the number of process cycles (purge–source–purge–$O_3$ = 5–4–5–3 [s]; 2 injections; 325 °C; Si wafer).

increasing $T_{dep}$ ranging from 200 °C to 375 °C. However, the trend appears divided into two regions: low $T_{dep}$ (200–275 °C) with a lower rate of increase in $G_r$, and high $T_{dep}$ (300–375 °C) with a higher rate of increase in $G_r$. It is believed that the low $T_{dep}$ region represents the genuine ALD region. At $T_{dep} > 300$ °C, the thermal decomposition of precursor molecules begins to contribute to the film deposition, and a higher $G_r$ increase with increasing $T_{dep}$ is observed. Although the growth at $T_{dep} < 300$ °C is closer to the genuine ALD reaction, the films in this study were grown at 325 °C to obtain a reasonable growth rate at that $T_{dep}$ (0.018 nm per cycle). Growth rates at $T_{dep} < 300$ °C were too low to be considered for mass production compatible DRAM capacitor dielectric processes. It should be noted that even above 300 °C, the growth rate is still lower than 0.25 Å per cycle. This means that the contribution of the self-decomposition to BTSO growth is small, which is supported by the self-limiting behavior of the film growth at 325 °C as shown in Figure 1b. If the films were mainly grown by the self-decomposition of the precursors, the growth rate should increase with the number of precursor injection without the saturation of the growth rate. Figure 1c shows that the film thickness increases linearly as the process cycles are repeated. The growth rate of BTSO films on bare Si substrates was determined to be ~0.018 nm per cycle from the slope of Figure 1c.

The as-deposited films grown at 325 °C are amorphous regardless of Si or Ru substrates. High-resolution transmission electron microscopy (HRTEM) image in Figure 2 shows a cross-section image of the BTSO film deposited on Ru at

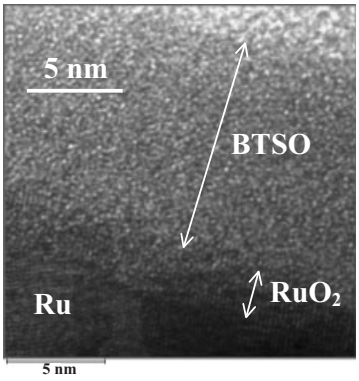


Fig. 2. HRTEM image of the BTSO film on a Ru substrate (purge–source–purge–$O_3$ = 5–4–5–3 [s]; 1 injection; 325 °C, 500 cycles).

325 °C, where no crystalline microstructure is observed. A very thin interfacial region (< 2 nm) shows some lattice fringes, which is possibly $RuO_2$ formed by the oxidation of the Ru surface during initial deposition cycles. An interfacial layer having lattice fringes was not observed in BTSO films on Si substrates. The average thickness of the $RuO_2$ interfacial layer and BTSO film were estimated to be ~1.5 nm and 11.7 nm, respectively, by X-ray reflectivity measurement.

Rutherford backscattering spectrometry (RBS) data, shown in Figure 3, shows that the cation ratio (Bi/Ti/Si) in the BTSO films on a Ru/$SiO_2$/Si substrate is 0.38:0.37:0.25. The rather high Si concentration probably results in the film

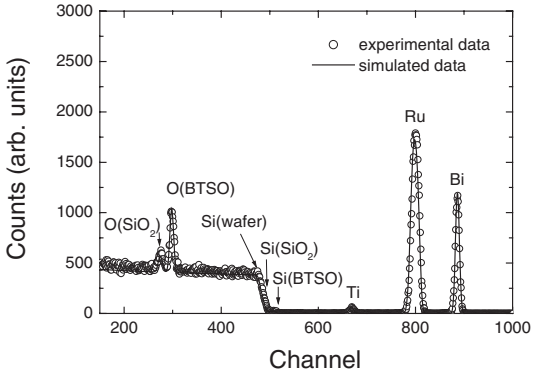


Fig. 3. RBS data for the BTSO film on Ru substrate (purge–source–purge–$O_3$ = 5–4–5–3 [s]; 2 injections; 325 °C, 600 cycles).

having an amorphous microstructure. Considering the molar ratio of the input precursor solution (Bi:Ti:Si = 3:16:16), Bi ions are ~5.3 times more efficiently incorporated to the BTSO film than Ti ions, even though they have the same ligand, mmp. Such a high incorporation of Bi can be explained by the lower charge-to-radius ratio of $Bi^{3+}$ (3.13) than that of $Ti^{4+}$ (5.88).[11] Since Bi shows a highly variable coordination number from 3 to 10 and an irregular coordination geometry,[12] the central Bi ion in $Bi(mmp)_3$ have unsaturated coordination sites which are electron deficient. Therefore, if there are some electron-donating groups on the growing surface such as hydroxyls or surface oxygens, the $Bi(mmp)_3$ can be more easily adsorbed on the surface than $Ti(mmp)_4$. Similar related results were also reported in the MOCVD of bismuth oxide and titanium oxide films wherein the growth rate of bismuth oxide from $Bi(mmp)_3$ is higher at low temperatures (below 350 °C) than that of titanium oxide from $Ti(mmp)_4$.[10]

Figure 4 shows the X-ray photoemission spectra (XPS) of $Bi_{4f}$, $Ti_{2p}$, $Si_{2p}$, and $O_{1s}$ core levels for an as-deposited BTSO film before and after the sputtering for 1 min using $Ar^+$ ions in the XPS chamber. Before the sputtering, the 5/2 and 7/2 spin-orbit doublet components of the $Bi_{4f}$ core level photoemission are located at 164.5 eV and 159.2 eV, respectively (Fig. 4a). The relative intensity ratio between $Bi_{4f_{5/2}}$ and $Bi_{4f_{7/2}}$ photoemission peaks is close to the theoretical ratio of 3:4, and the energy spacing between the peaks is 5.3 eV. The line shape of the $Bi_{4f}$ core level photoemission changes with sputtering, which is consistent with reports on $Bi_2Ti_2O_7$, $Bi_4Ti_3O_{12}$ and their La-doped films.[13] After sputtering, an additional spin-orbit doublet emerges at the low binding energy side of the spectra, slightly overlapping the major $Bi_{4f}$ photoemission peaks. The areas of low binding energy peaks of $Bi_{4f}$ photoemission increase from ~1 % of the main peak area before sputtering to ~7.7 % after the 1 min sputtering, as shown in Figure 4a. These new

  

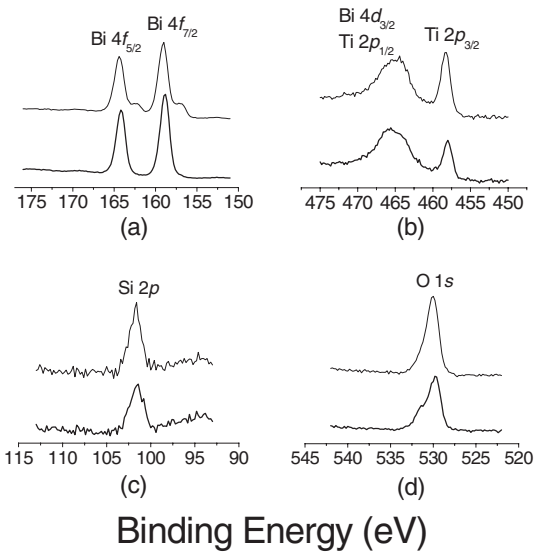


Fig. 4. Core level photoemission spectra of BTSO: a) $Bi_{4f}$; b) $Ti_{2p}$; c) $Si_{2p}$; d) $O_{1s}$. The thick and thin spectra are obtained from the as-received and 1 min sputtered film, respectively. (Purge–source–purge–$O_3$ = 5–4–5–3 [s]; 2 injections; 325 °C, 600 cycles).

peaks are assigned to the metallic bismuth peak that is formed by the Bi-O bond breaking and oxygen release during the sputtering process.[13]

The $Ti_{2p_{1/2}}$ photoemission peak partially overlaps the $Bi_{4d_{3/2}}$ core level peak (Fig. 4b). The $Ti_{2p_{3/2}}$ photoemission peak is located at 458.3 eV as a distinctively resolved feature. The binding energy of $Ti_{2p_{3/2}}$ core level is close to those reported for $TiO_2$, which range from 458.33 eV to 459.0 eV. The $Si_{2p}$ photoelectron peak appears at the binding energy of 101.8 eV, which is lower than that of $SiO_2$ (Fig. 4c). The line shape of the $O_{1s}$ core level photoemission reveals that the peak is composed of two components (Fig. 4d). The first peak at the low binding energy side possibly originates from the oxygen bonded to Bi, Ti, and/or Si, while the second one near ~531.7 eV is ascribed to hydrocarbon contamination, since the second peak disappears after the sputtering.

Table 1 summarizes the binding energies of core electrons in BTSO and its related compounds. The binding energies of $Bi_{4f}$ and $Si_{2p}$ electrons are different from those of bismuth titanates and silicon dioxide. These shifts indicate that the chemical states of the grown BTSO films are not simply described by the physical mixture of separate phases consisting of simple binary oxides such as $Bi_2O_3$, $TiO_2$, $SiO_2$ and Bi-containing compounds.

Figure 5 shows the XPS depth profile of each element in the BTSO film. The silicon and oxygen compositions are almost constant throughout the thickness of the BTSO film. However, the bismuth composition decreases and titanium composition increases with increase in depth. Such an inverse depth profile of Bi and Ti is unusual and is probably tainted by the sputtering. Since metallic bismuth formed by sputtering is moderately volatile in high vacuum (~$10^{-4}$ torr at 520 °C),[17] the Ti concentration can be higher for the sputtered surface in comparison with the as-received one. The oxygen concentration in the depth profile is ~62 %, and carbon was not detected except for surface contamination even after sputtering for 6 min. It should be noted that the $C_{1s}$ peak overlaps the $Ru_{3d}$ core level peak so that the carbon profile is denoted with the same symbol as that for Ru in Figure 5.

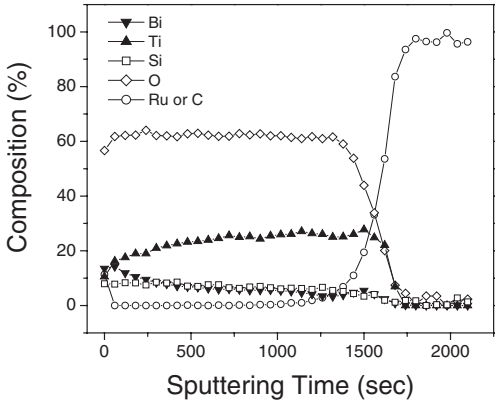


Fig. 5. The depth profile of the as-deposited BTSO thin film on a Ru substrate by XPS. (Purge–source–purge–$O_3$ = 5–4–5–3 [s]; 2 injections; 325 °C, 600 cycles).

The film step coverage in terms of thickness and composition were investigated using a patterned wafer having rectangular-shaped holes with a depth of 1200 nm and an opening of 300 nm that were etched in a $SiO_2$ layer, as shown in Figure 6a. The BTSO film was deposited at 325 °C with a precursor dose of two injections for 1000 cycles. The thickness step coverage was >90 % as seen by the magnified inset images. The compositional uniformity in the hole was investigated with depth profiles, which was obtained by scanning the cross section of the specimen from the surface of the film to the interface of BTSO/$SiO_2$ using TEM-EDS (energy disper-

Table 1. Binding energies of various compounds related to BTSO.

| Compound | Binding energy [a] [eV] | | | | | |
|---|---|---|---|---|---|---|
| | Bi | | Ti | Si | O | Ref. |
| | $4f_{5/2}$ | $4f_{7/2}$ | $2p_{3/2}$ | 2p | 1s | |
| $Bi_2O_3$ | 165.1 | 159.8 | | | 530.2 | 14 |
| $TiO_2$ | | | 458.3 | | 529.9 | 15 |
| $SiO_2$ | | | | 103.5 | 532.8 | 15 |
| $Bi_2Ti_2O_7$ | 165.1 | 159.7 | | | | 16 |
| $Bi_4Ti_3O_{12}$ | 163.8 | 158.4 | 458.1 | | | 13 [b] |
| Bi | 162.0 | 156.7 | | | | 14 |
| BTSO [b] | 164.5 | 159.2 | 458.3 | 101.8 | 530.0 | |
| | 164.7 | 159.4 | 458.6 | 102.0 | 530.4 | |

[a] The binding energies were referenced to $C_{1s}$ at 284.8 eV. [b] The upper and lower row values were obtained from as-received and 10 min sputtered films, respectively.

  

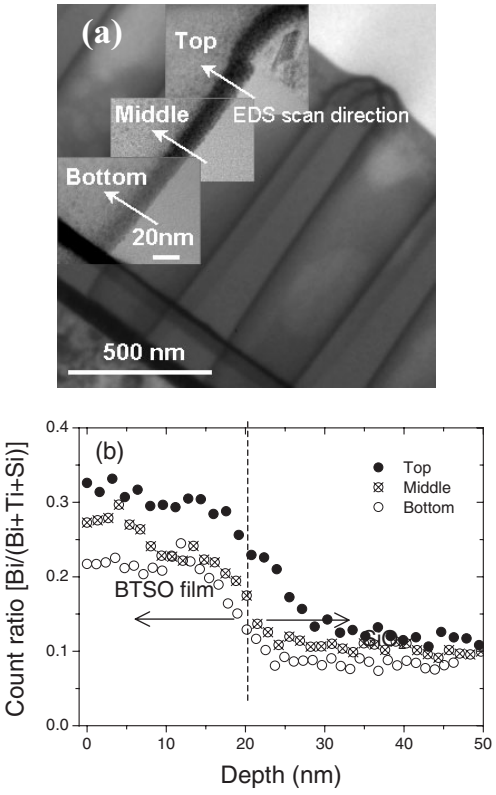


Fig. 6. a) TEM images and b) compositional uniformity of the BTSO film deposited on the $SiO_2$ substrate patterned with rectangular holes. (purge–source–purge–$O_3$ = 5–4–5–3 [s]; 2 injections; 325 °C, 1000 cycles).

sive spectroscopy). The EDS experiments were performed at the top (●), middle (⊗) and bottom (○) of the hole. Figure 6b shows that the count ratio of Bi ion and total cations (Bi+Ti+Si) in the BTSO film decreases from the top to bottom region of the hole. Such non-uniformity of the Bi content in a hole is probably ascribed to an insufficient dose of $Bi(mmp)_3$ and/or its thermal decomposition that can occur at high deposition temperatures above the ALD window.

The electrical properties of a BTSO film, 13 nm thick, was measured with Pt (100 nm)/BTSO/Ru (100 nm) capacitors. The capacitor area was determined by the Pt top electrode area which was formed using a shadow mask (hole diameter = 300 μm). The leakage current density of the BTSO films is $< 10^{-8}$ A cm$^{-2}$ at 1 V, as shown in Figure 7, which is low enough for current DRAM capacitor applications.[1c] The leakage current increases more rapidly for the negative voltage sweep than for the positive one suggesting inferior properties of the top Pt/BTSO interface to those of the bottom Ru/BTSO interface. A mild annealing at 440 °C in vacuum (~ 1.2 torr) results in a more symmetrical current–voltage curve shape. However, the annealing process results in degraded leakage current characteristics with an abrupt leakage increase above 1.3 V. This may be due to oxygen vacancies generated by vacuum annealing.

From capacitance–voltage measurements at 10 kHz, the dielectric constant and dielectric loss factor (tan$\delta$) of the as-

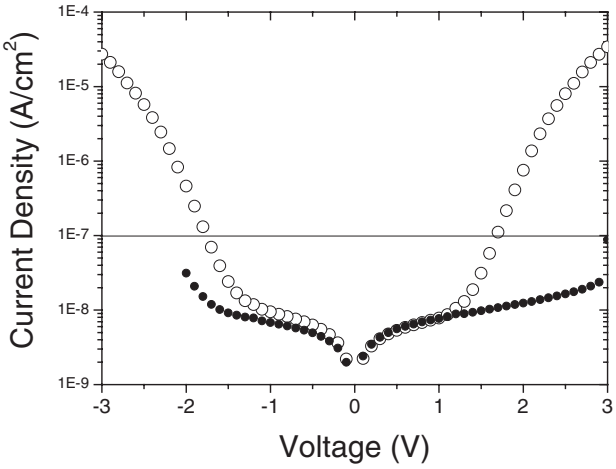


Fig. 7. *I–V* characteristics of planar BTSO capacitors [Pt (100 nm)/BTSO (13 nm, 600 cycles)/Ru (50 nm)/$SiO_2$ (45 nm)/Si] before (●) and after (○) 440 °C annealing. (Purge–source–purge–$O_3$ = 5–4–5–3 [s]; 2 injections; 325 °C, 600 cycles).

deposited BTSO film were 24 and 0.0068, respectively. After vacuum annealing, the dielectric constant and dielectric loss factor slightly deteriorated to 21 and 0.0113, respectively, possibly due to oxygen vacancies generated by vacuum annealing. It was observed that the photoemission peak from the metallic bismuth became stronger for the vacuum annealed film than for the as-deposited one.

The equivalent oxide thicknesses ($t_{ox}$), of the as-deposited and vacuum annealed film were 2.1 nm and 2.4 nm, respectively. The term $t_{ox}$ represents the theoretical thickness of $SiO_2$ that would be required to achieve the same capacitance density obtained from a high-*k* dielectric capacitor. It should be noted that the amorphous BST or ST ($SrTiO_3$) films usually show a similar dielectric constant (~ 20)[18] with low leakage current density. However, with post-annealing, these amorphous film easily crystallized to a polycrystalline film with large grain sizes and many pores that result in a large leakage current.[19] The BTSO films in this study remained amorphous and low leakage current properties were retained after post-annealing.

## 3. Conclusion

An alternative high-*k* material, amorphous $Bi_{1-x-y}Ti_xSi_yO_z$ (BTSO) thin films and its ALD process were studied for its application as a DRAM capacitor dielectric. BTSO films grown by ALD showed good step coverage in high aspect ratio structures. The leakage current density of BTSO films (13 nm thick) is $< 10^{-8}$ A cm$^{-2}$ at 1 V, which is low enough to be used as a DRAM capacitor dielectric. The dielectric constant of the amorphous BTSO films was estimated to be ~ 24 ($t_{ox}$ = ~ 2.1 nm) from the *C–V* characteristics at 10 kHz of a Pt/BTSO/Ru capacitor.

  

## 4. Experimental

*Metal Precursors and Oxidant Gas*: $Bi(mmp)_3$, $Ti(mmp)_4$, and $Si(OEt)_4$ [mmp = 1-methoxy-2-methyl-2-propoxide ($OCMe_2CH_2OMe$, Me = methyl); Et = ethyl] were dissolved in ethylcyclohexane to obtain the precursor solution with the ratio of Bi/Ti/Si = 3:16:16. The concentrations of Bi, Ti and Si precursors were 15 mM, 80 mM, and 80 mM, respectively. Ozone gas with a concentration of 150 g $m^{-3}$ was generated by an Ozonizer.

*ALD System and Procedures*: A liquid delivery technique with a single cocktail solution was adopted in this study for the stable and precise supply of complex precursors. The single cocktail precursor solution was contained in a canister that was pressurized with Ar gas in order to deliver the precursor solution into a liquid injector. The liquid injector was connected to a vaporizer which was attached to a reaction chamber. The vaporizer temperature was kept at 200 °C. When the injector was turned on, about 0.028 mL of the precursor solution was injected and the precursor vapors were carried by an Ar gas (300 sccm) to the ALD chamber. The valves for the precursor vapor and ozone gas (300 sccm) were alternately opened and closed for 4 s and 3 s, respectively, with a spacing of 5 s to purge out volatile by-products and any excess reactants in the reaction chamber by the purge Ar gas (1300 sccm). Diluted Ar gas at 1000 sccm was introduced during the oxidant gas and precursor feeding steps for sufficient dispersion of the reaction gases over the entire wafer surface. The working pressure was regulated to about 1 torr in every step by an automatic valve.

*Thin Film Characterization*: The film thickness was determined by a spectroscopic ellipsometer (J. A. Woollam Co., Inc.) with a Cauchy dispersion model. XRR measurements were carried out in a $\theta$–$2\theta$ scan mode using a Philips X'pert pro MRD X-ray diffractometer with Cu K$\alpha$ radiation. Low-angle XRR data was collected with 0.002° increments and 2 s count times. XRR data were analyzed with the WinGixa program, provided by Philips. TEM images and EDS data were obtained by a TECNAI-UT30 microscope equipped with a Schottky-type field emission gun operating at 300 kV. XPS spectra were measured on a Quantum 200 Scanning Microprobe spectrometer using a monochromatic Al K$\alpha$ emission. Sputtering during the XPS was performed with 0.5 keV $Ar^+$ ions. The film composition was determined from RBS spectra obtained with a NEC6-SDH spectrometer with a helium ion beam of 2.0 MeV. RBS data simulation was performed using the RUMP software from Computer Graphic Service (CGS).

*Electrical Measurements*: Pt top electrodes (100 nm thick) were deposited on the BTSO/Ru/$SiO_2$/Si samples with a shadow mask (hole diameter = 300 μm) by DC magnetron sputtering. *I–V* and *C–V* characteristics were measured using a Keithley 236 Source Measurement Unit and a Precision LCR Meter (HP 4284A) at 10 kHz, respectively.

Received: June 23, 2004
Final version: August 2, 2004

[1] a) C. S. Hwang, *Mater. Sci. Eng. B* **1998**, *56*, 178. b) A. I. Kingon, J.-P. Maria, S. K. Streiffer, *Nature* **2002**, *406*, 1032. c) Semiconductor Industry Association, *International Technology Roadmap for Semiconductor* **2001**, <http://public.itrs.net/>

[2] a) Y. K. Park, C. H. Cho, K. H. Lee, B. H. Roh, Y. S. Ahn, S. H. Lee, J. H. Oh, J. G. Lee, D. H. Kwak, S. H. Shin, J. S. Bae, S. B. Kim, J. K. Lee, J. Y. Lee, M. S. Kim, J. W. Lee, D. J. Lee, S. H. Hong, D. I. Bae, Y. S. Chun, S. H. Park, C. J. Yun, T. Y. Chung, K. Kim, *2002 IEEE International Electron Devices Meeting (IEDM 2002) Technical Digest*, IEEE, Piscataway, NJ **2002**, p. 819. b) W. D. Kim, J. H. Joo, Y. K. Jeong, S. J. Won, S. Y. Park, S. C. Lee, C. Y. Yoo, S. T. Kim, J. T. Moon, *2001 IEEE International Electron Devices Meeting (IEDM 2001) Technical Digest*, IEEE, Piscataway, NJ **2001**, p. 263.

[3] M. Nayak, S. Ezhilvalavan, T. Y. Tseng, in *Handbook of Thin Film Materials*, Vol. 3 (Ed: H. S. Nalwa), Academic Press, San Diego, CA **2002**, Ch. 2.

[4] a) D. J. Otway, W. S. Rees, Jr., *Coord. Chem. Rev.* **2000**, *210*, 279. b) M. Tiitta, L. Niinisto, *Chem. Vap. Deposition* **1997**, *3*, 167.

[5] a) K. Natori, D. Otani, N. Sano, *Appl. Phys. Lett.* **1998**, *73*, 632. b) C. T. Black, J. J. Welser, *IEEE Trans. Electron Dev.* **1999**, *46*, 776. c) C. S. Hwang, *J. Appl. Phys.* **2002**, *92*, 432.

[6] C. S. Hwang, S. Y. No, J. Park, H. J. Kim, H. J. Cho, Y. K. Han, K. Y. Oh, *J. Electrochem. Soc.* **2002**, *149*, G585.

[7] a) L. W. Fu, H. Wang, S. X. Shang, X. L. Wang, P. M. Xu, *J. Cryst. Growth* **1994**, *139*, 319. b) X. Wu, S. W. Wang, H. Wang, Z. Wang, S. X. Shang, M. Wang, *Thin Solid Films* **2000**, *370*, 30. c) S. W. Wang, H. Wang, X. Wu, S. Shang, M. Wang, Z. Li, W. Lu, *J. Cryst. Growth* **2001**, *224*, 323.

[8] M. Ritala, M. Leskela, in *Handbook of Thin Film Materials*, Vol. 1 (Ed: H. S. Nalwa), Academic Press, San Diego, CA **2002**, Ch. 2.

[9] W. A. Herrmann, N. W. Huber, O. Runte, *Angew. Chem. Int. Ed. Engl.* **1995**, *34*, 2187.

[10] A. C. Jones, P. A. Williams, N. L. Tobin, P. R. Chalker, P. Marshall, P. J. Wright, P. A. Lane, P. Donohue, L. M. Smith, H. O. Davies, *Electrochem. Soc. Proc.* **2003**, *2003-08*, 871.

[11] *CRC Handbook of Chemistry and Physics*, CRC Press, Boca Raton, FL **2000**, 12-1.

[12] M. N. Sokolov, T. V. Mitkina, O. A. Gerasko, V. P. Fedin, A. V. Virovets, R. Llusar, *Z. Anorg. Allg. Chem.* **2003**, *629*, 2440.

[13] a) Y. Zhang, H. Wang, S. X. Shang, X. H. Xu. X. N. Yang, W. M. Liu, *Mater. Lett.* **2004**, *58*, 1056. b) C. Jovaleckic, M. Pavlovic, P. Osmokrovic, L. Atanasoska, *Appl. Phys. Lett.* **1998**, *72*, 1051. c) M. W. Chu, M. Ganne, M. T. Caldes, E. Gautier, L. Brohan, *Phys. Rev. B* **2003**, *68*, 14 102.

[14] V. Dharmadhikari, S. R. Sainkar, S. Badrinarayan, A. Goswami, *J. Electron Spectrosc. Relat. Phenom.* **1982**, *25*, 181.

[15] R. P. Netterfield, P. J. Martin, C. G. Pacey, W. G. Sainty, D. R. McKenzie, G. Auchterlonie, *J. Appl. Phys.* **1989**, *66*, 1805.

[16] W. E. Morgan, W. J. Stec, J. R. Van Wazer, *Inorg. Chem.* **1973**, *12*, 953.

[17] E. B. Graper, J. Vossen, in *Handbook of Thin Film Process Technology* (Eds: D. A. Glocker, S. Shah), Institute of Physics Publishing, Bristol, UK **1995**, Part A, Ch. 1.

[18] H. Kawano, K. Morii, Y. Nakayama, *J. Appl. Phys.* **1993**, *73*, 5141.

[19] C. S. Hwang, S. O. Park, C. S. Kang, H. J. Cho, H. K. Kang, S. T. Ahn, M. Y. Lee, *Jpn. J. Appl. Phys. Part 1* **1995**, *34*, 5178.

  